

Spectral dependence of radiative horizontal transport in stratocumulus clouds and its effect on near-IR absorption

E. I. Kassianov

Pacific Northwest National Laboratory, Richland, Washington, USA

Y. L. Kogan

Cooperative Institute for Mesoscale Meteorological Studies, University of Oklahoma, Norman, Oklahoma, USA

Received 16 January 2002; revised 19 July 2002; accepted 8 September 2002; published 11 December 2002.

[1] The spectral dependence of the radiative horizontal transport (the horizontal transport of radiative energy) E and its effect on the accuracy of spectral and broadband absorption retrieval in the near-infrared (IR) wavelength range was investigated using a large-eddy simulation (LES) cloud model with explicit microphysics and a three-dimensional Monte Carlo radiative transfer model. Two typical types of marine clouds representing inhomogeneous overcast and broken stratocumulus clouds have been simulated. We demonstrate that (1) the basic statistics (e.g., variance and correlation function) of the horizontal transport are wavelength-dependent and (2) the estimates of spectral and broadband absorption with a given accuracy (e.g., $rmse \sim 4\%$) may require the use of different spatial resolutions. **INDEX TERMS:** 3210 Mathematical Geophysics: Modeling; 3359 Meteorology and Atmospheric Dynamics: Radiative processes; 3360 Meteorology and Atmospheric Dynamics: Remote sensing; **KEYWORDS:** radiative horizontal transport, cloud inhomogeneity, spectral and broadband absorption

Citation: Kassianov, E. I., and Y. L. Kogan, Spectral dependence of radiative horizontal transport in stratocumulus clouds and its effect on near-IR absorption, *J. Geophys. Res.*, 107(D23), 4712, doi:10.1029/2002JD002103, 2002.

1. Introduction

[2] The amount of shortwave absorption and its space-time variability is a fundamental factor governing weather and climate. The formulation of shortwave absorption in climate models is quite challenging due to extreme cloud inhomogeneities and difficulties in representing them on a large-scale grid. Cloud absorption estimates, based on model calculations and field measurements, may substantially disagree [see, e.g., Rawlins, 1989; Stephens and Tsay, 1990; Ramanathan et al., 1995; Arking, 1996; Cess et al., 1995, 1999], and this cannot be explained clearly and unambiguously yet. The identification and explanation of possible causes for the discrepancy have been targeted in a large body of theoretical and experimental research, as well as field campaigns such as the Atmospheric Radiation Measurement (ARM) Enhanced Shortwave Experiments (ARESE) (see, e.g., <http://www.arm.gov/docs/iops/arese/>).

[3] Two traditional methods have been used to estimate the cloud absorption from measurements of vertical fluxes. The first method is based on the solar cloud forcing at the surface level and at the top of the atmosphere [Ramanathan et al., 1995], and the second method is based on the analysis of the slope of the linear regression between albedo and transmittance [Cess et al., 1995]. Both these two methods neglect horizontal radiative fluxes. Hereafter we will use the term “horizontal transport” to describe the net radiative

energy transport in the horizontal directions. The effect of the horizontal transport on the accuracy of the absorption retrievals is an active area of research [e.g., Barker and Li, 1997; Marshak et al., 1997, 1999a, 1999b; Titov, 1998]. In particular, Marshak et al. [1997] and Titov [1998] (hereinafter referred to as M97 and T98, correspondingly) performed detailed sets of theoretical computations and showed that the horizontal transport is comparable with the vertical fluxes and absorption at small (~ 0.1 km) scales. As a result, these two methods [Ramanathan et al., 1995; Cess et al., 1995] provide a significant bias in absorption estimation at small scales. Therefore spatial averaging (over at least ~ 6 km) should be applied to get a reliable estimation of cloud absorption. In addition, M97 and T98 also showed that the averaging scale depends on the solar zenith angle (SZA) and the horizontal cloud variability.

[4] A method that allows one to obtain absorption estimates of high spatial resolution (~ 0.1 km) was proposed by Ackerman and Cox [1981]. It is based on simultaneous measurements of net vertical fluxes in the visible and near-IR wavelength ranges and consists of two steps. First, the value of horizontal transport at a wavelength outside the absorption band (e.g., in the visible range) is determined. Second, this value is used to estimate cloud absorption in the near-IR spectral range. In other words, it is implied that horizontal transport depends weakly on wavelength. This method and its different modifications have been frequently used to determine the absorption in inhomogeneous clouds [see, e.g., Hayasaka et al., 1995a; Titov and Kasjanov, 1997; T98; M97; Marshak et al., 1999a]. The objective of

the present work is to investigate the spectral dependence of the horizontal transport (in terms of the basic statistics) and its effect on the broadband horizontal transport. We also estimate the maximum spatial resolution with which one can retrieve the spectral and broadband cloud absorption.

[5] Although the present work and some of the previous ones [Titov and Kasjanov, 1997; T98; M97; Marshak et al., 1997, 1999a, 1999b] are based on similar philosophies—dealing with a theoretical study of the spectral variability of 3-D radiative effects—they are very different. Below we outline four main distinctions between the previous papers and our current one. First, we compute both the spectral horizontal transport (313 spectral subintervals) and the broadband horizontal transport (0.7–2.7 μm), while previous work presented radiative calculations for given sets of the single scattering albedo (water droplet absorption) [e.g., Titov and Kasjanov, 1997; T98; Marshak et al., 1999a, 1999b] or for a single spectral subinterval (0.91–1.0 μm) with strong water vapor absorption [M97]. Second, we study the individual and combined effect of the water vapor absorption and water droplet absorption on the spectral behavior of the horizontal transport. Third, we compare the effect of scattering and absorbing properties of a cloudy atmosphere on the spectral variability of the horizontal transport. Finally, we apply more realistic three-dimensional (3-D) cloud fields with detailed microphysics. We discuss these distinctions in more detail in section 2. In section 3 we describe briefly models of marine stratocumulus clouds and the simulation method. Section 4 presents calculations of the horizontal transport in the visible and near-IR spectral range. The effect of the spectral variability of the horizontal transport on the accuracy of absorption retrieval is discussed in section 5. A summary of this work is given in section 6. The Monte Carlo technique is described in Appendix A.

2. A Brief Review of Various Modifications of the Ackerman-Cox Method

[6] A number of modifications of the Ackerman-Cox method have been developed recently. Marshak et al. [1999a] (hereinafter referred to as M99a) have suggested the following two modifications of the Ackerman and Cox method. The first modification (subtraction modification) involves a deconvolution of derived cloud absorption (by using traditional Ackerman and Cox method) with a gamma-approximation of the radiative-transfer Green function. This approximation is a two-parameter gamma-type distribution [Marshak et al., 1995; Davis et al., 1997]. The first parameter (the characteristic radiative smoothing scale) η is closely related to $\langle \rho \rangle$, where $\langle \rho \rangle \approx h[\tau(1 - g)]^{-1/2}$ (albedo case) and $\langle \rho \rangle \approx h$ (transmittance case); h is the geometrical cloud thickness, τ is the cloud optical depth ($\tau = h\sigma$, σ -extinction coefficient) and g is the asymmetry factor of the scattering function. The second parameter α is equal to $\langle \rho \rangle^2 \text{var}(\rho)^{-1}$, where $\text{var}(\rho) = \langle \rho^2 \rangle - \langle \rho \rangle^2$. In other words, the spectral features of the gamma-approximation are specified by cloud scattering properties (σ , g). Therefore, the subtraction modification relies (indirectly, through the gamma-approximation) on the assumption that the spectral dependence of the horizontal transport is governed by scattering properties of clouds only. In the second modification (conditional sampling), the cloud absorption

is derived for only those pixels (columns) that have small horizontal fluxes in a transparent band. To put it differently, it was assumed that if the horizontal flux is small in a nonabsorbing spectral band, then it should be small in an absorbing spectral band as well. Note, M99a have performed calculations for six single-scattering albedos that represent typical values in the shortwave wavelength range.

[7] The sensitivity of the horizontal transport and its three components (reflected, transmitted and absorbed photons) to the single scattering albedo, ω_0 , has been estimated by Marshak et al. [1999b] (hereinafter referred to as M99b). M99b have shown that the magnitude of horizontal transport increases with the decrease of ω_0 . The magnitude of the horizontal transport, E , has been measured as $\|E\| = [\int |E(x)|^2 dx]^{1/2}$, where L is the outer scale or the size of the basic cloud cell (pixel). In addition, M99b have studied the sensitivity of this magnitude to SZA and the averaging scale.

[8] Titov and Kasjanov [1997] have performed calculations of the horizontal transport for two different values of the single scattering albedo ($\omega_0 = 1$ and $\omega_0 = 0.99$) and have shown, that (1) a linear regression describes quite accurately the functional relation between the horizontal transport values in nonabsorbing ($\omega_0 = 1$) and absorbing ($\omega_0 = 0.99$) bands, and (2) the slope (multiplying coefficient) of the linear regression is greater than one. Based on these findings, another modification of the Ackerman-Cox method (the linear regression modification) has been suggested [Titov and Kasjanov, 1997]: instead of replacing the horizontal transport in an absorbing band by the horizontal transport in a nonabsorbing band, a linear regression between the nonabsorbing and absorbing values of the horizontal transport has been applied. This linear regression modification yields an improved estimation of water droplet absorption [Titov and Kasjanov, 1997; T98] in overcast stratocumulus clouds. For broken stratocumulus clouds, M97 have shown that using the linear regression between absorption (interval 0.91–1.0 μm) and apparent absorption in an almost transparent subinterval (around 0.99 μm) allows one to improve the water vapor absorption estimation. Note that all these findings [Titov and Kasjanov, 1997; T98; M97] are limited to one-dimensional fractal models (vertically uniform cloud extinction coefficient depends on the single horizontal coordinate) with plane-parallel geometry and uniform microphysics. Since solar fluxes and cloud absorption are sensitive to the horizontal and vertical cloud structure and internal variation of microphysical properties [e.g., Li et al., 1994; Barker et al., 1999], here we use 3-D cloud fields with detailed microphysics (see next section).

[9] Also, it was previously demonstrated [Titov and Kasjanov, 1997; T98] that the regression slope is sensitive to the SZA and surface albedo; for all values of SZA and surface albedo considered, the slope is greater than one. This means that the magnitude of the horizontal transport in an absorbing band (water droplets absorption) can be larger than the horizontal transport in a nonabsorbing band (conservative scattering). This result is in line with M99b findings. The original physical explanation of this spectral dependence has been advanced in T98: the absorption by water droplets increases the number of photon trajectories that contribute to the horizontal transport.

[10] The present work further explores the spectral variability of the horizontal transport and addresses the following specific questions: How does the regression slope depend on the wavelength? What factors (e.g., the scattering, absorption) responsible for this spectral dependence are most important? Is the regression slope always greater than one? Since the regression slope is a function of variance and correlation coefficient [see, e.g., *Freund and Minton*, 1979], we include these traditional statistics in our analysis (sections 4 and 5). Note that the variance of the horizontal transport $var(E)$ determines the amplitude of E fluctuations (magnitude of E), and the correlation coefficient $\rho(E_{vis}, E_{ir})$ measures the degree of linear dependence between values of the horizontal transport in visible E_{vis} and near-IR E_{ir} spectral range. Furthermore, the accuracy of absorption retrieval is a function of spatial resolution [e.g., T98; M97]. This brings up the question: Is the spatial resolution the same for the spectral and broadband absorption retrievals? To address this issue, we include in our analysis the correlation function of E (or the correlation radius Δl^*) as well (sections 4 and 5). Note, the correlation radius Δl^* determines the spatial scale of E fluctuations. We evaluate the spectral variability of the horizontal transport E in terms of the variance $var(E)$, the correlation radius Δl^* and the correlation coefficient $\rho(E_{vis}, E_{ir})$. The spectral values of $var(E)$ and $\rho(E_{vis}, E_{ir})$ are used to determine the variance of broadband horizontal transport $var(E_{broad})$ (section 4b) and spectral values of the regression line slope (section 5). The linear regression between E_{ir} and E_{vis} is applied for the absorption retrieval (section 5).

3. Approach

[11] Originally the Ackerman and Cox method was suggested for the 0.3–2.8 μm spectral interval [*Ackerman and Cox*, 1981]. In this wavelength range, the spectral variation of the horizontal transport is governed by spectral variability of cloud, as well as aerosol and underlying surface optical properties. For our study, we chose the spectral interval 0.7–2.7 μm , where one can neglect the spectral variability of the molecular scattering (the latter is more pronounced in the shorter spectral range 0.3–0.7 μm [see, e.g., *Liou*, 1992]). The optical depth of marine aerosol is small, and therefore its influence was ignored as well. Since the ocean albedo is roughly wavelength independent for the selected spectral interval [*Soulen et al.*, 2000], the spectral behavior of the horizontal transport in marine stratocumulus is determined mainly by the cloud and atmospheric gases properties. Note that for surfaces resembling green vegetation the horizontal transport depends strongly on the spectral behavior of the surface albedo [*Barker and Marshak*, 2001].

[12] The marine stratocumulus clouds produced in the study are simulated by a tool known as a large eddy simulation (LES) model with a fairly detailed representation of physical processes in the cloud-topped marine boundary layer. The Cooperative Institute of Mesoscale Meteorological Studies (CIMMS) LES model couples the 3-D dynamics with explicit formulation of cloud physics processes based on prediction equations for cloud condensation nuclei and cloud drop spectra [*Kogan et al.*, 1995]. The LES results have been thoroughly verified against observations of boundary layer dynamics, turbulence, microphysical, and radiative param-

eters and have demonstrated good agreement with observational data [*Khairoutdinov and Kogan*, 1999]. We simulated two marine stratus cloud layers observed on June 12, 1992, during the Atlantic Stratocumulus Transition Experiment (ASTEX) field campaign. The first cloud layer represents a solid stratocumulus cloud deck, while the second one represents a broken stratocumulus cloud field (Figure 1). The broken stratus cloud evolved in a clean air mass with moderate drizzle (0.5–1.0 mm/day). Due to drizzle, the cloud base and top were highly inhomogeneous with cloud base varying from 150 to 300 m and the cloud top from 700 to 775 m. The maximum cloud top height was the same for both the broken and overcast cloud fields and equaled 775 m. The minimum cloud base height was 150 m and 225 m for the broken and overcast cloud fields, respectively. Note that the lateral boundary conditions are periodic; as a result, the simulated broken cloud field represents so-called “cloud streets” with cloud fraction varying from approximately 0.1 near the surface to 0.7 at the upper levels.

[13] The integration domain of $3 \times 3 \text{ km}^2$ consists of $40 \times 40 \times 51$ grid points with a horizontal and vertical resolution of 75 m and 25 m, respectively. Above the simulation domain, the atmosphere is represented by a set of horizontally homogeneous layers with different geometrical thicknesses, corresponding to vertical levels used in atmospheric general circulation models [see, e.g., *Ellingson et al.*, 1991]. The pressure, temperature, and concentration of water vapor were selected to match the midlatitude summer conditions of the ASTEX experiment.

[14] The cloud optical properties (the extinction coefficient σ , the single scattering coalbedo $1-\omega_0$ and the scattering function g) were calculated based on Mie theory using drop size distributions predicted by the LES model. The absorption by atmospheric gases was obtained by calculating transmission functions for water vapor and carbon dioxide (see Appendix A), which in the lower atmosphere and the selected spectral interval (0.7–2.7 μm) are the most important atmospheric absorbers [*Goody and Yung*, 1989]. The carbon dioxide mixing ratio was specified at 365 ppm. The mean vertical profiles of water vapor and the extinction coefficient (Figure 2) are quite different for broken and overcast cloud cases resulting in a large difference between optical depths in these two cases (Figure 3a).

[15] The spectral absorption A_λ^* , the vertical upwelling flux $F_{\lambda,top}^\uparrow$ at the cloud top and the downwelling flux $F_{\lambda,base}^\downarrow$ at the cloud base for each vertical column in the integration domain was calculated using the Monte Carlo method (see Appendix A). The fluctuations of the horizontal transport increase as the solar zenith angle increases [see, e.g., M97; T98]. To evaluate the nearly maximum influence of the horizontal transport on cloud absorption retrieval, all calculations were performed for a solar zenith angle of 60° . With 100 million photons used in calculations, the mean computational error was within 1%. The net radiative horizontal flux $F_{\lambda,hrz}$, lost ($F_{\lambda,hrz} > 0$) or gained ($F_{\lambda,hrz} < 0$) through the column sides was calculated from radiative energy conservation:

$$F_{\lambda,top}^\uparrow + F_{\lambda,base}^\downarrow + A_\lambda^* + F_{\lambda,hrz} = F_{\lambda,top}^\downarrow \quad (1)$$

[16] Note that the left side of (1) does not contain the term $F_{\lambda,base}^\uparrow$. Since the effect of the surface albedo and

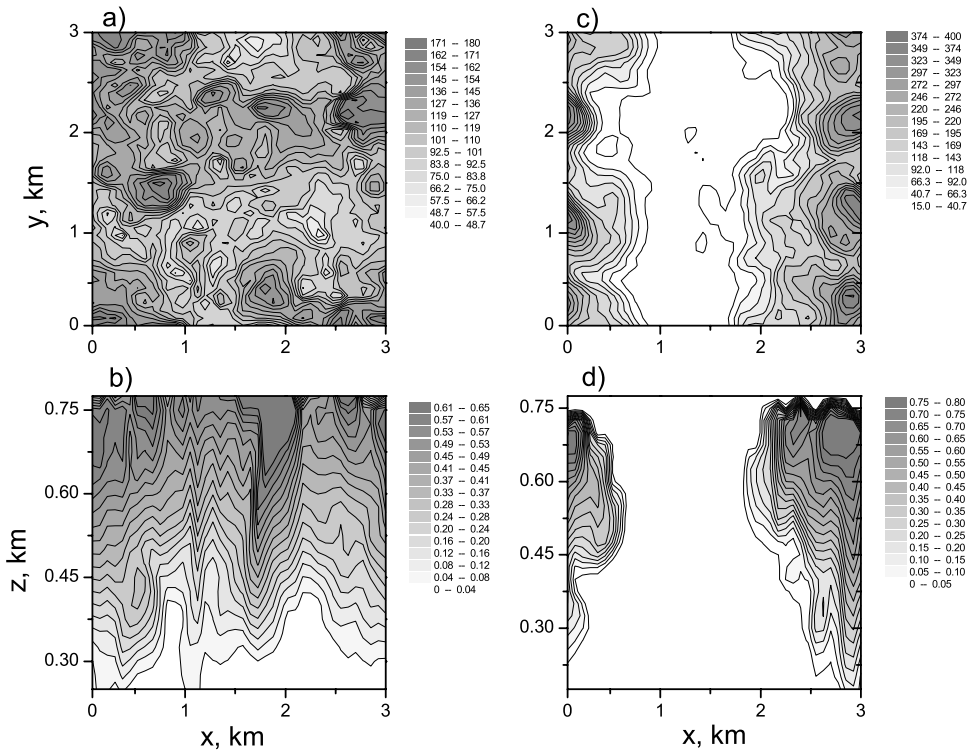


Figure 1. (a, c) The horizontal cross sections of liquid water path, g/m^2 ; (b, d) the vertical cross sections ($y = 1.5 \text{ km}$) of liquid water content, g/m^3 for overcast (a, b) and broken (c, d) cloud field.

aerosol is neglected, $F_{\lambda, \text{base}}^{\uparrow} = 0$. In addition to the spectral calculations, the broadband ones were performed over the selected spectral interval $0.7\text{--}2.7 \mu\text{m}$. The latter was divided into M subintervals with spectral resolution of 20 cm^{-1} ($M = 313$). The same resolution was used to calculate the spectral dependence of all parameters.

[17] The spectral variability of both the extinction coefficient and the asymmetry factor is weak (Figure 3). The relative effect of about 10% increase of the asymmetry factor in the $2.5\text{--}2.7 \mu\text{m}$ subinterval on the broadband radiative transfer is insignificant, since the solar irradiance in this subinterval is small [see, e.g., *Liou, 1992*]. Thus, we neglect the spectral variability of the extinction coefficient and the asymmetry factor in the broadband radiative calculations. The single scattering coalbedo, however, can vary by several orders of magnitude (Figure 3c), therefore its wavelength dependence was taken into account.

4. Spectral and Broadband Radiative Horizontal Transport

4.1. Spectral Variability of Horizontal Transport

[18] We define the spectral horizontal transport as $E_{\lambda} = F_{\lambda, \text{hzt}}^{\uparrow} / F_{\lambda, \text{top}}^{\uparrow}$. Our calculations show that for integration domain of $3 \times 3 \text{ km}^2$ the mean value of E is zero for all wavelengths. Therefore, we use the variance $\text{var}(E_{\lambda})$, correlation coefficient $\rho(E_{\lambda_1}, E_{\lambda_2})$ and correlation function $C_{\lambda}(\Delta l)$ (where Δl is the horizontal distance) of the horizontal transport to evaluate spectral variability of E_{λ} (section 4.1). Also we link these spectral statistics with broadband ones (section 4.2) and discuss the accuracy of the spectral and broadband absorption retrievals (section 5).

The linear regression modification (see section 2) is used for these retrievals.

[19] As is well known, the water vapor and water droplet bands contribute most to cloud absorption and vertical fluxes in the near-IR range. What is the difference of horizontal transport in these two bands? To answer this question we compare its parameters at three wavelengths: $0.7 \mu\text{m}$ (pure scattering, no water vapor absorption), $0.94 \mu\text{m}$ (strong water vapor absorption) and $1.65 \mu\text{m}$ (strong cloud droplet absorption). It is worth noting that observations at $0.94 \mu\text{m}$ and $1.65 \mu\text{m}$ bands are commonly used for retrieval of cloud geometrical thickness [*Hayasaka et al., 1995b*] and cloud droplet effective radius [*Asano et al., 1995*].

[20] The *Ackerman and Cox* [1981] method assumes that (1) the horizontal transport depends mainly on the scattering properties (σ and g), and (2) the latter are wavelength-independent. The second assumption is physically well grounded, while the first is less evident. Numerous theoretical and experimental studies [see, e.g., *Deirmendjian, 1969*; *Goody and Yung, 1989*] suggest that the cloud scattering properties (σ and g) may vary by 2–5% per micrometer of wavelength, while the single scattering coalbedo, $1 - \omega_0$, and absorption coefficient of atmospheric gases and water vapor may vary by several orders of magnitude. Thus, one might expect that spectral behavior of absorbing properties may have a stronger influence on horizontal transport than scattering ones. This will be verified in the following two sets of tests. In the first, we neglected absorption by water vapor and droplets, but considered the spectral variations of σ and g by assigning them different values at three wavelengths, 0.7 , 0.94 , and $1.65 \mu\text{m}$. The second set of tests was similar to the first, except that the

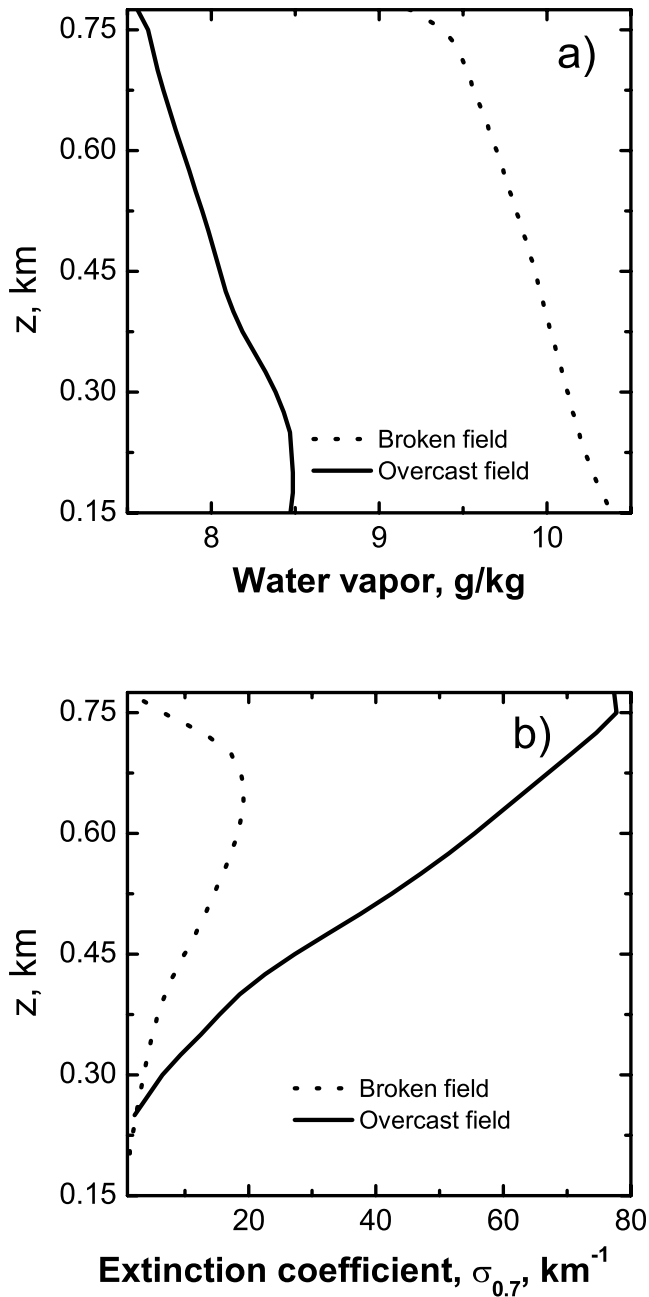


Figure 2. The vertical profiles of (a) the domain-averaged water vapor mixing ratio, and (b) the domain-averaged extinction coefficient at $0.7 \mu\text{m}$, for the broken (dashed) and overcast (solid lines) cloud fields.

absorption by water vapor and droplets was also taken into account.

[21] Figure 4 shows the results of the first set of tests. Although the horizontally averaged horizontal transport is zero, each grid cell can gain (negative values of E) or lose (positive E) radiative energy through its sides. Compared to the overcast case, the broken field is more inhomogeneous (Figure 1); therefore in this case, the fluctuations of E are significantly larger (note difference in scales). The range of these fluctuations (for both the overcast and broken cases) is similar to the one obtained earlier for typical overcast [e.g.,

T98, Figure 5] and broken [e.g., M99a, Figure 12] inhomogeneous clouds. Note that even for the overcast inhomogeneous clouds, the neglect of E would cause considerable errors in the absorption estimations [e.g., T98]. For a broken marine stratocumulus cloud considered here, a substantial portion of unscattered radiation may propagate in gaps. At the base of the cloud, the value of unscattered radiation for some pixels is equal to 1, because the direction toward the Sun is not obscured by clouds. For these pixels, the values of total transmittance (unscattered plus diffuse radiation) may exceed 1 due to the additional contribution of diffuse radiation, resulting in $|E| > 1$. Let us now discuss another difference between the fluctuations of E in broken and overcast cloud fields. For the overcast field, (1) the number of positive and negative values of E is about the same, and (2) the maximum amplitudes of E fluctuations are roughly equal in magnitude in negative $|E_{\min}|$ and positive E_{\max} directions (relative to the mean value, $\langle E \rangle = 0$). This means that for the overcast case, the one-point probability density of E has a near symmetric shape. For the broken field, due to the unscattered radiation contribution, the tail of one-point probability density of E extends toward the negative end of the scale, and $|E_{\min}| > E_{\max}$ (negatively skewed

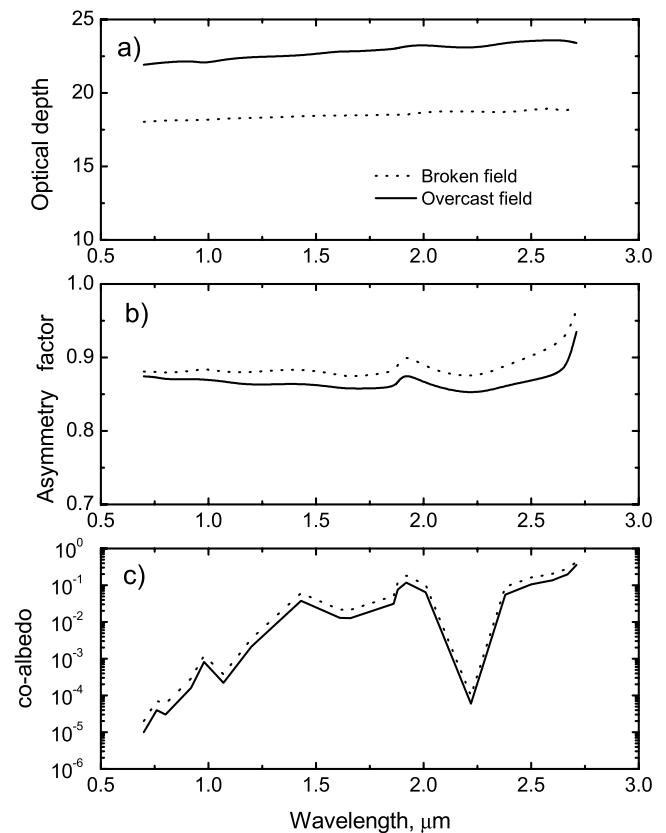


Figure 3. The spectral dependence of (a) optical depth, (b) asymmetry factor, and (c) single scattering coalbedo, $1 - \omega_0$, averaged over domain. The mean optical depth of broken clouds is more than 3 times less than the mean optical depth of the overcast clouds. To ease the comparison of the spectral dependence of these optical depths, the optical depth of the broken cloud field (dashed line) is multiplied by a factor of 3.

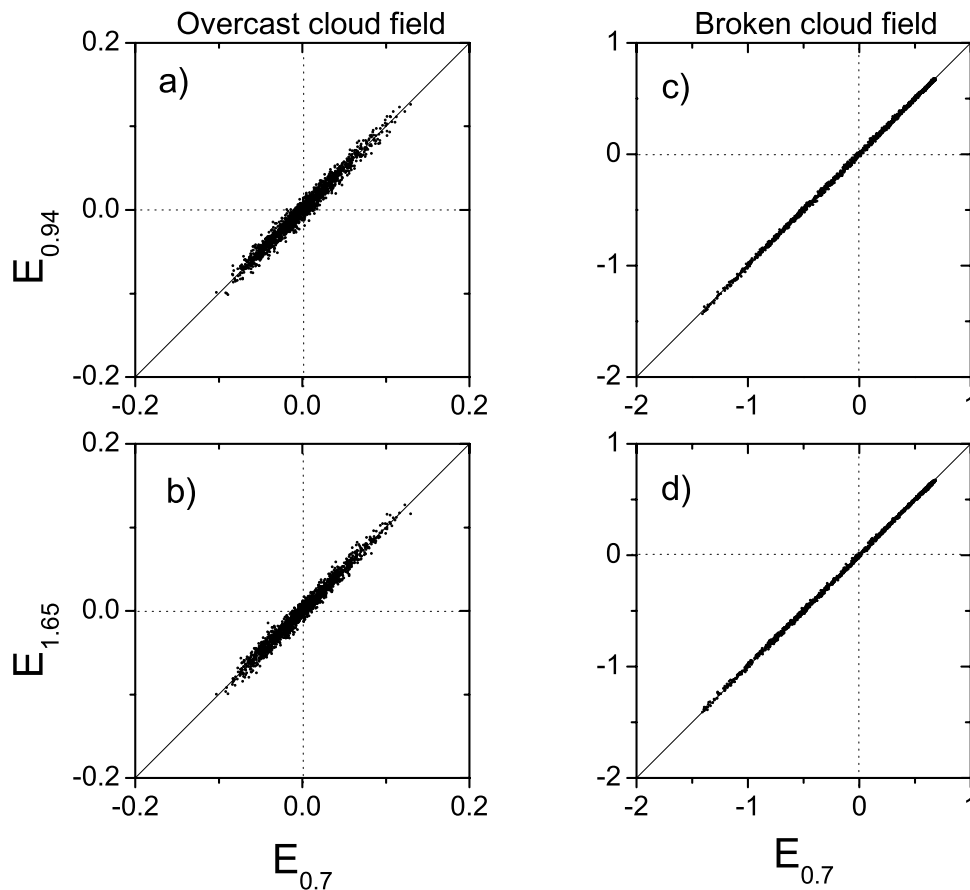


Figure 4. The comparison of horizontal transport E for the case without absorption in the overcast (left panels) and broken cloud field (right panels) experiments: (a, c) comparison of E in the visible ($E_{0.7}$) versus water vapor spectral band ($E_{0.94}$); (b, d) comparison of E in the visible ($E_{0.7}$) versus water droplet spectral band ($E_{1.65}$). (Note, that E is dimensionless.)

distribution). Figure 4 clearly shows the high correlation between values of E at three different wavelengths, thus confirming that spectral dependence of scattering parameters is negligible.

[22] In the second set of tests we considered absorption by water vapor and droplets as well. Before making quantitative estimates, let us evaluate the dependence of E on absorption qualitatively. In an arbitrary pixel the E value can be expressed in terms of the number of photons crossing lateral pixel sides and their statistical weight, which is proportional to photon energy. For instance, if the left pixel side is crossed by N_+ photons in the positive X direction, each with the same statistical weight W_{in} , and by N_- photons in the negative X direction, each with the statistical weight W_{out} , the horizontal transport E (at the left pixel side) will be equal to $N_+W_{in} - N_-W_{out}$. The products N_+W_{in} and N_-W_{out} characterize the flux density of radiation through the pixel side in the positive and negative X directions. In the general case, photons may have different statistical weights.

[23] How may absorption influence the number of photons contributing to E and their statistical weight? Suppose that a photon entered the pixel through its left-hand side, underwent a scattering within it, and left the pixel through the same pixel side. In this case, $N_+ = N_- = 1$, and the contribution of the photon trajectory segment to E is $\Delta E = W_{in} - W_{out}$, where W_{in} and W_{out} are photon statistical

weights at the entry and exit points. In the absence of either gaseous or droplet absorption, $W_{in} = W_{out}$, as a result this photon makes no contribution to E . In the presence of absorption, however, W_{out} is less than W_{in} and contribution of this photon to E is $\Delta E = W_{in} - W_{out}$. Thus, the presence of absorption can increase the number of photon trajectories contributing to E [T98].

[24] Let us consider another possible situation, in which a photon has traveled a geometrical path l and has undergone n collisions before entering the pixel through its left-hand side, but left the pixel through its bottom. In this case, $N_+ = 1$, $N_- = 0$, the contribution of this photon trajectory segment to the horizontal transport is $\Delta E = W_{in}$. Obviously, either gaseous absorption (proportional to the geometrical path l) or droplet absorption (proportional to the order of photon scattering n) decreases W_{in} , resulting in ΔE value that will be less in the absorptive than in the nonabsorptive case. The presence of absorption can decrease the weight of the photon contributing to E . Thus, these two competing effects, which are associated with the number of photons contributing to E and their statistical weight, will determine the differences between E values in nonabsorptive and absorptive bands. In particular, these two effects define the spectral variability of E fluctuations (their magnitude and spatial scale).

[25] Table 1 shows the values of $var(E_\lambda)$ at three different wavelengths. In the overcast cloud case, $var(E_{1.65})$ is nearly

Table 1. Variance of the Spectral and Broadband Horizontal Transport $var(E)$ in the Overcast and Broken Cloud Field Cases

Variance	Overcast Case	Broken Case
$var(E_{0.7})$	0.00133	0.295
$var(E_{0.94})$	0.00134	0.252
$var(E_{1.65})$	0.00302	0.353
$var(E_{broad})$	0.00202	0.315

twice the value of $var(E_{0.7})$, apparently due to water droplet absorption. Therefore, the water droplet absorption can significantly increase the amplitude of E fluctuations. This is consistent with previous findings [e.g., T98; M99b]. The correlation coefficient $\rho(E_{0.7}, E_{1.65})$ is about 0.8 (Table 2). The water vapor absorption influences the horizontal transport weakly: $var(E_{0.7})$ and $var(E_{0.94})$ almost coincide and the value of $\rho(E_{0.7}, E_{0.94})$ is close to 1 (Table 2). In contrast to the overcast case, in the broken case a considerable contribution to E may come from unscattered radiation, passing in gaps between clouds. Therefore, any difference in spectral behavior of E between overcast and broken cases can primarily be attributed to this unscattered component. The unscattered radiation does not depend on the droplet absorption, and so it is the same at both $0.7 \mu\text{m}$ and $1.65 \mu\text{m}$. This is why the relative difference between $var(E_{0.7})$ and $var(E_{1.65})$ is smaller for the broken case than for overcast one (Table 1). For the same reason, the correlation between $E_{0.7}$ and $E_{1.65}$ is stronger (Table 2). The water vapor absorption decreases the unscattered component, which, in turn, leads to a decrease of $var(E_{0.94})$ and the inequality $var(E_{0.94}) < var(E_{0.7})$ is valid (Table 1).

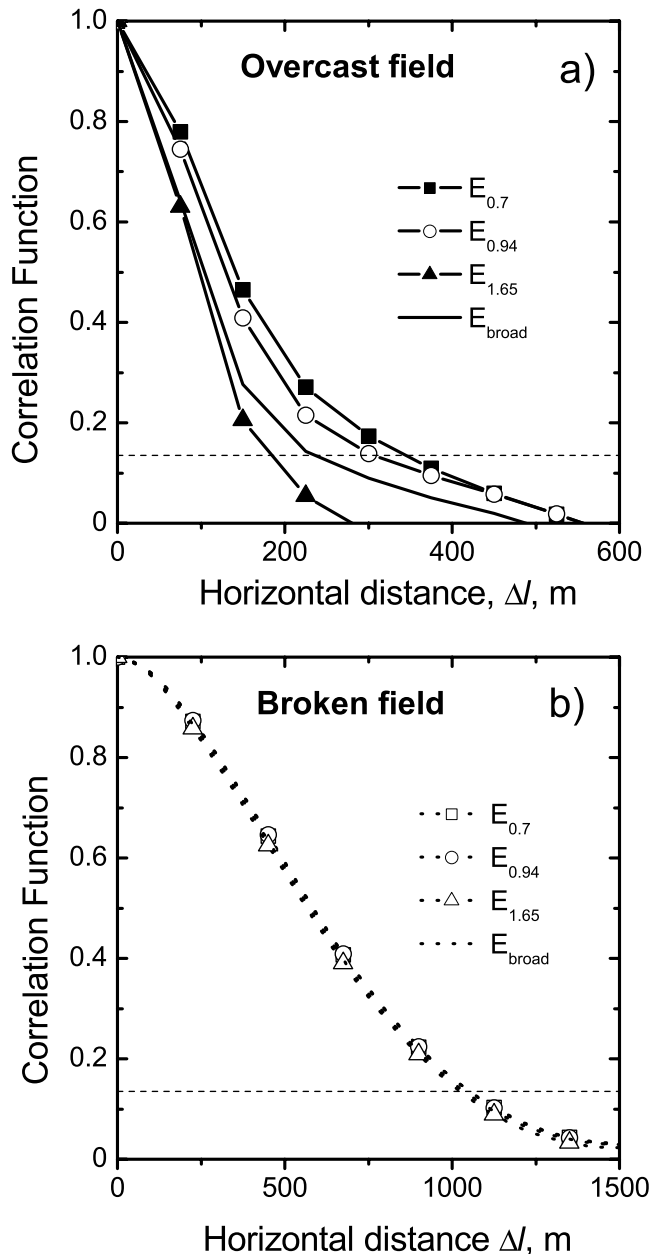
[26] Let us consider the normalized autocorrelation function, $C_\lambda(\Delta l)$, of the horizontal transport E_λ , where Δl is the horizontal distance. Recall, the variance $var(E_\lambda)$ characterizes the amplitude of E_λ fluctuations, and $C_\lambda(\Delta l)$ characterizes their spatial scale. If the autocorrelation $C_\lambda(\Delta l)$ drops rapidly as Δl increases, then E_λ has small-scale variability. And vice versa, if $C_\lambda(\Delta l)$ drops slowly as Δl increases, then E_λ has large-scale variability. Commonly, the correlation radius (the value $\Delta l = \Delta l^*$, where $C_\lambda(\Delta l^*)$ is small) determines the characteristic spatial scale of E_λ fluctuations. In other words, two arbitrary pixels have almost uncorrelated values E_λ if they are located $\sim \Delta l^*$ and more apart. In our analysis, we determine the correlation radius as Δl^* value, where $C_\lambda(\Delta l^*) = e^{-2} = 0.1353$. To estimate the one-dimensional (horizontal) autocorrelation $C_\lambda(\Delta l)$ from the two-dimensional (x- and y-coordinates) field of E_λ , we have performed (analogously to Varnai [2000]) the following two-step data processing procedure. First, we determined the autocorrelation $C_\lambda(\Delta l)$ for each row in two directions (along-Sun and cross-Sun), and then we averaged (variance-weighted average) these autocorrelations. Figure 5 shows the autocorrelations $C_\lambda(\Delta l)$ for both the overcast and broken fields. It is easily seen that, for the broken field, Δl^* is significantly larger than Δl^* for the overcast field. Thus, for the broken field, E_λ has large-scale variability; for the overcast field, the opposite is true. These findings are in harmony with those of other investigators [see, e.g., T98; M97; M99b].

[27] Let us discuss the new results regarding the spectral dependence of Δl^* . For the overcast field, the absorption can decrease the correlation radius considerably (about two

Table 2. Correlation Coefficient ρ Between Horizontal Transport at Various Wavelengths for Overcast and Broken Cloud Field Cases

Correlation Coefficient	Overcast Case	Broken Case
$\rho(E_{0.7}, E_{0.94})$	0.973	0.999
$\rho(E_{0.7}, E_{1.65})$	0.781	0.994
$\rho(E_{0.7}, E_{broad})$	0.876	0.998

times) (Figure 5a). This can be explained as follows. As geometrical distance (optical depth) between the given pixel and its neighbor increases, both the order of photon scattering and the total photon path length increase. Therefore, photons leaking out the horizontal sides of a given pixel can

**Figure 5.** Normalized correlation functions of the spectral ($E_{0.7}$, $E_{0.94}$, $E_{1.65}$) and broadband (E_{broad}) horizontal transport for overcast (a) and broken (b) cloud fields.

interact effectively with its neighbors that are located $\sim \Delta l^*$ or less apart. The contribution of these photons to the neighbor's horizontal transport decreases because of the water droplet absorption (proportional to the mean order of photon scattering) and the water vapor absorption (proportional to the total photon path length). As a result, for a given geometrical distance and the scattering properties, the contribution decreases as absorption increases. In other words, as absorption grows (geometrical distance and the scattering properties are fixed), the statistical interrelation between E_λ values at the two different pixels (separated at a fixed distance) gets weaker and results in a decrease of Δl^* . As discussed earlier (Figure 4), for the broken field the unscattered radiation contributes significantly to the E_λ fluctuations. Since this unscattered component (1) is independent of water droplet absorption and (2) is diminished slightly by water vapor, the correlation radius Δl^* has a weak spectral dependence for the broken field (Figure 5b).

[28] The absorption by water vapor and cloud droplets may have opposite influences on the spectral horizontal transport. For example, for broken clouds the cloud droplet absorption at $\lambda = 1.65 \mu\text{m}$ can increase the variance of horizontal transport, $\text{var}(E)$, by 20%, while the water vapor absorption at $\lambda = 0.94 \mu\text{m}$ can decrease, $\text{var}(E)$ by 15% (Table 1). Thus, it can be suggested that the net effect of the water vapor and cloud droplets on the broadband horizontal transport E_{broad} may be less than their individual effect on the spectral horizontal transport (see next subsection).

4.2. Broadband Horizontal Transport

[29] The broadband horizontal transport can be written as

$$E_{broad} = \sum_{k=1}^M a_k E_k, \quad (2)$$

where a_k and E_k are the weight and the value of the spectral horizontal transport, respectively.

[30] From (2) it follows that the variance of the broadband horizontal transport $\text{var}(E_{broad})$ can be written as [Feller, 1971]

$$\text{var}(E_{broad}) = \sum_{k=1}^M a_k^2 \text{var}(E_k) + 2 \sum_{j,k} a_j a_k \rho(E_j, E_k) \sqrt{\text{var}(E_j)} \sqrt{\text{var}(E_k)}, \quad (3)$$

where the last sum is taken over each of the pairs (E_j, E_k) with $j < k$.

[31] From (3) it is evident that for given values of a_k , the variance of the broadband horizontal transport $\text{var}(E_{broad})$ is a function of both the variances $\text{var}(E_k)$ and correlation coefficient $\rho(E_j, E_k)$ between values of the horizontal transport at different wavelengths. Note that the covariance is defined to be $\text{Cov}(E_j, E_k) = \rho(E_j, E_k) \sqrt{\text{var}(E_j)} \sqrt{\text{var}(E_k)}$ [Feller, 1971]. The first term in (3) represents the weighted sum of spectral variances $\text{var}(E_k)$, which are proportional to the spectral amplitudes of E_k . The second term describes the weighted sum of corresponding spectral covariances $\text{Cov}(E_j, E_k)$, which measure the direction and magnitude of the relationship between the spectral values E_j and E_k .

[32] It follows from (2)–(3) that $E_{broad} = E_{vis}$ and $\text{var}(E_{broad}) = \text{var}(E_{vis})$ if the horizontal transport is spec-

trally independent. However, as statistics for three wavelengths shown in Table 1 illustrate, approximate equality $\text{var}(E_{broad}) \approx \text{var}(E_{vis})$ may hold if for some wavelengths $\text{var}(E_k) > \text{var}(E_{vis})$, but for others $\text{var}(E_k) < \text{var}(E_{vis})$. For example, for the broken case, the value of $\text{var}(E_\lambda)$ is larger than $\text{var}(E_{0.7})$ at $\lambda = 1.65 \mu\text{m}$, but smaller at $\lambda = 0.94 \mu\text{m}$. Therefore small differences found between E_λ magnitudes (e.g., the small differences between $\text{var}(E_{broad})$ and $\text{var}(E_{vis})$) cannot be considered an indication that the horizontal transport has a weak spectral dependence.

[33] Similar to the variance $\text{var}(E_{broad})$, the normalized autocorrelation function of the broadband horizontal transport, $C_{broad}(\Delta l)$, can be written as

$$C_{broad}(\Delta l) = \frac{1}{\text{var}(E_{broad})} \sum_{k=1}^M a_k^2 \text{var}(E_k) C_k(\Delta l) + \frac{2}{\text{var}(E_{broad})} \sum_{j,k} a_j a_k C_{j,k}(\Delta l) \sqrt{\text{var}(E_j)} \sqrt{\text{var}(E_k)}, \quad (4)$$

where $C_{j,k}(\Delta l)$ is the normalized cross-correlation function between $E_j(x)$ and $E_k(x + \Delta l)$; $C_{j,k}(\Delta l)$ can be interpreted as a measure of the “similarity” between a realization $E_j(x)$ and a shifted realization $E_k(x + \Delta l)$. Note, if $\Delta l = 0$, then $C_{j,k}(0) = \rho(E_j, E_k)$, $C_k(0) = 1$, and $C_{broad}(0) = 1$.

[34] It follows from Equations (3)–(4) that the relative contribution of the spectral correlation functions $C_k(\Delta l)$ and $C_{j,k}(\Delta l)$ to the broadband correlation function $C_{broad}(\Delta l)$ is determined by the corresponding contribution of the spectral variances to the broadband variance $\text{var}(E_{broad})$. For the cloud fields considered here, the following inequalities hold (Figure 5): $\Delta l^*_{1.65} < \Delta l^*_{broad} < \Delta l^*_{0.94} < \Delta l^*_{0.7}$. It means, that the horizontal scale of E_{broad} fluctuations is smaller than the corresponding scale of $E_{0.7}$ fluctuations. For the overcast field, both the spectral value, $\Delta l^*_{1.65}$, and broadband one, Δl^*_{broad} , diverged considerably from $\Delta l^*_{0.7}$ (Figure 5a) (e.g., $\Delta l^*_{broad} \sim 0.6 \Delta l^*_{0.7}$). For the broken field, both the spectral $\Delta l^*_{0.94}$, $\Delta l^*_{1.65}$ and broadband Δl^*_{broad} values of the correlation radius are comparable with $\Delta l^*_{0.7}$ (Figure 5b). Thus, we reach the following conclusion: the spectral variability of the correlation radius Δl^* is more pronounced in the overcast field; for the broken field, the spectral changes of Δl^* can be neglected.

[35] In the general case, the statistics of the broadband horizontal transport (e.g., the variance, correlation radius) can depend in a complex way on SZA, the cloud optical and geometrical (e.g., the cloud top height) parameters, as well as on the concentration of water vapor in the cloudy atmosphere.

5. Horizontal Transport and Absorption Retrieval

[36] Let us consider the effect of the spectral dependence of E on the accuracy of the absorption retrieval. It follows from the radiative energy conservation law that the absorption A can be determined from the measured albedo R , transmittance T and horizontal transport E . The horizontal transport, however, is difficult to measure, so its effect on RT is usually neglected (as, e.g., in the independent pixel approximation). Numerous studies, however, showed that

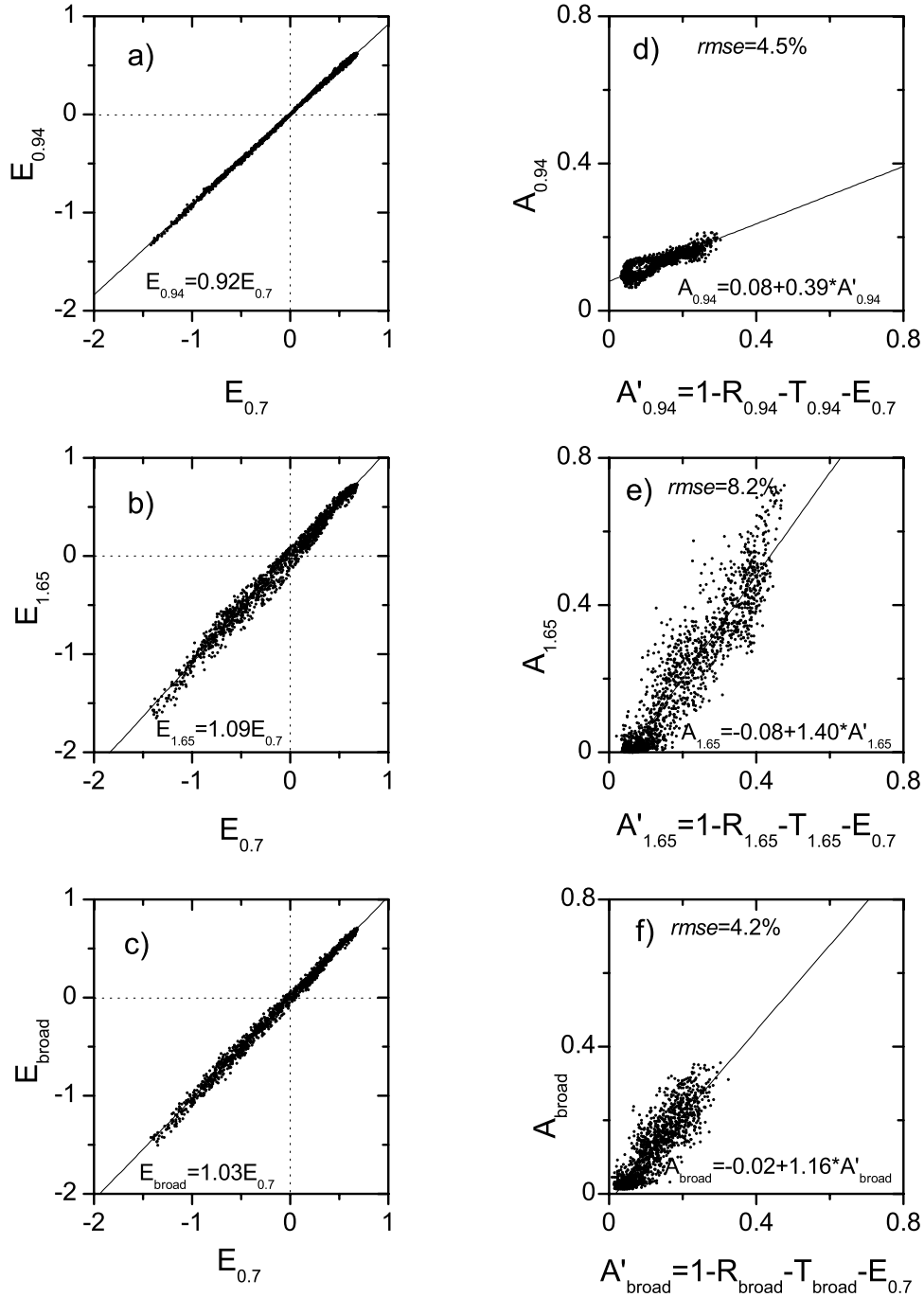


Figure 6. The horizontal transport (a, b, c) and the real A and reconstructed absorption A' (d, e, f) for small (75 m) spatial scale in the broken cloud field. (a) $E_{0.7}$ vs $E_{0.94}$; (b) $E_{0.7}$ vs $E_{1.65}$; (c) $E_{0.7}$ vs E_{broad} ; (d) $A_{0.94}$ vs $A'_{0.94}$, (e) $A_{1.65}$ vs $A'_{1.65}$ and (f) A_{broad} vs A'_{broad} .

neglect of E may result in unrealistic cloud absorption estimates at small (of the order of 100 m) spatial scales [see, e.g., M97; T98; Hayasaka *et al.*, 1995a; Rawlins, 1989]. Also it was demonstrated that the accuracy of cloud absorption retrievals can decrease significantly as fluctuations of the horizontal transport increase. For broken clouds, the variance $var(E)$ exceeds by approximately two orders of magnitude the variance $var(E)$ for overcast clouds (Table 1). Therefore, for broken clouds, the effect of E on the accuracy of cloud absorption retrieval is also larger. We thus use the broken case as an example of the effect of E on the

absorption retrieval in the IR interval. Next, we discuss the errors of spectral/broadband absorption retrieval versus the averaging spatial scale for both types of cloud (broken and overcast cloud fields).

[37] Ackerman and Cox [1981] proposed a method that accounts for horizontal transport in cloud absorption retrievals. It determines E in the visible range $E_{vis} = 1 - R_{vis} - T_{vis}$ and uses this value for estimating infrared absorption $A_{ir} = 1 - R_{ir} - T_{ir} - E_{vis}$. In other words, it is assumed that E_{vis} is equal to E_{ir} . Figure 6 shows that E_{vis} and E_{ir} are approximately linearly related, and a

Table 3. Slope (Multiplying Factor) of the Linear Regression Between Horizontal Transport at Various Wavelengths for Overcast and Broken Cloud Field Cases

Multiplying Factor	Overcast Case	Broken Case
$E_{0.94} = bE_{0.7}$	0.97	0.93
$E_{1.65} = bE_{0.7}$	1.18	1.09
$E_{broad} = bE_{0.7}$	1.08	1.03

straight line (the linear regression) provides an appropriate description of the data. This is consistent with previously reported results obtained for one-dimensional fractal cloud models [see, e.g., M97; T98]. Two factors will determine the accuracy of the absorption retrieval: (1) the slope of the scatterplot, and (2) the degree to which the points in the scatterplots cluster about a straight line representing

the slope. The slope of the linear regression can be defined as the product of the correlation coefficient $\rho(E_{vis}, E_{ir})$ and the standard deviation $\sqrt{var(E_{ir})}$ divided by the standard deviation $\sqrt{var(E_{vis})}$ [see, e.g., Freund and Minton, 1979]. Because of the spectral variations of $var(E)$ and $\rho(E_{vis}, E_{ir})$ (see previous section), the slope can deviate from 1 (Figure 6 and Table 3). Note that the slope depends on both wavelength and cloud type. To quantify the accuracy of prediction A from A' (absorption retrieval) for the whole domain, we will use the corresponding root-mean-square (*rms*) errors. These are defined as a square root of the sum $\frac{1}{n} \sum_{i=1}^n (A(i) - A'(i))^2$, where n is the number of points in the scatterplots.

[38] Let us illustrate the effect of these two factors on the absorption retrieval. First, we compare the real absorption A

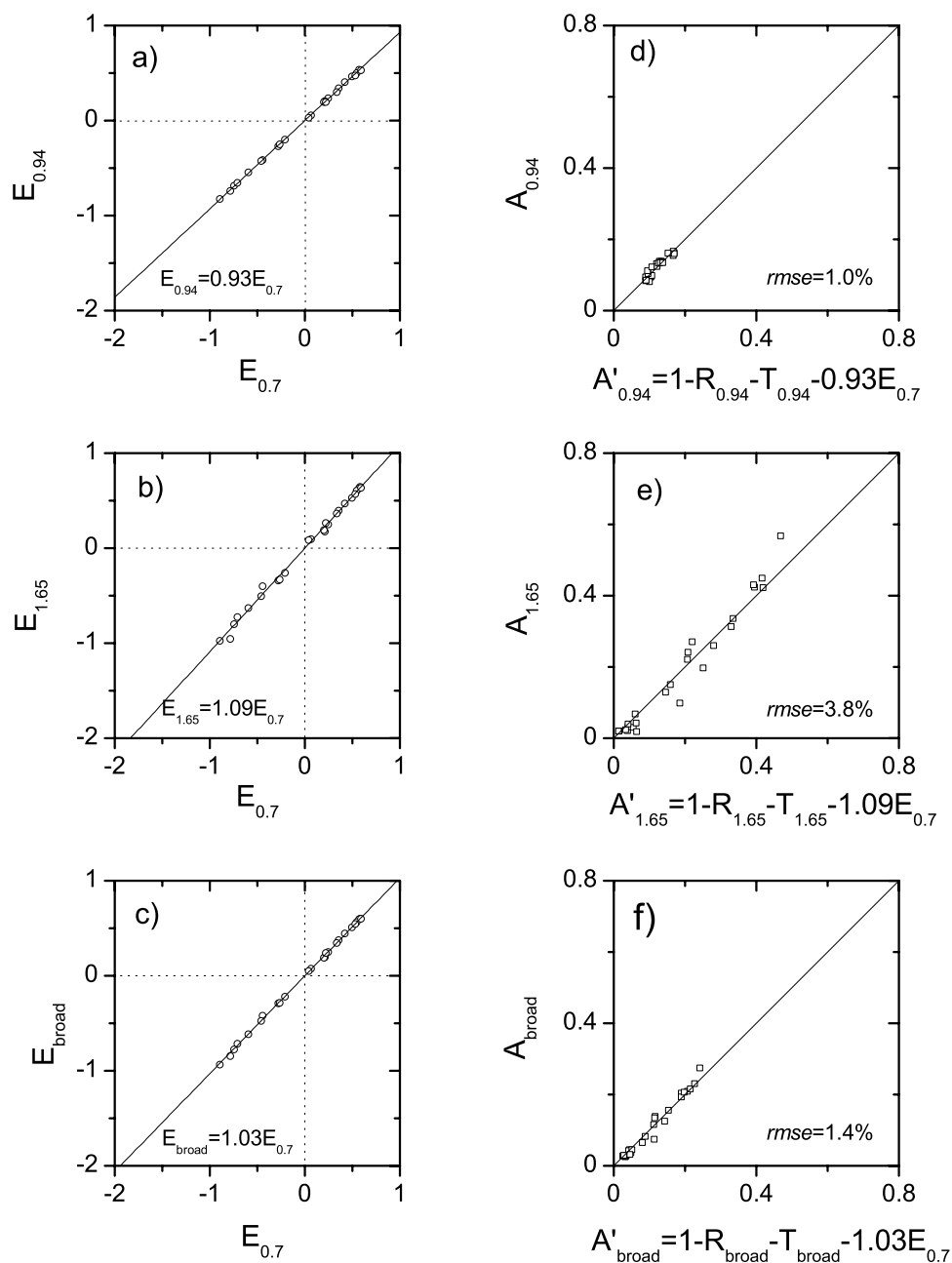


Figure 7. The same as Figure 6, but for large (600 m) spatial scale.

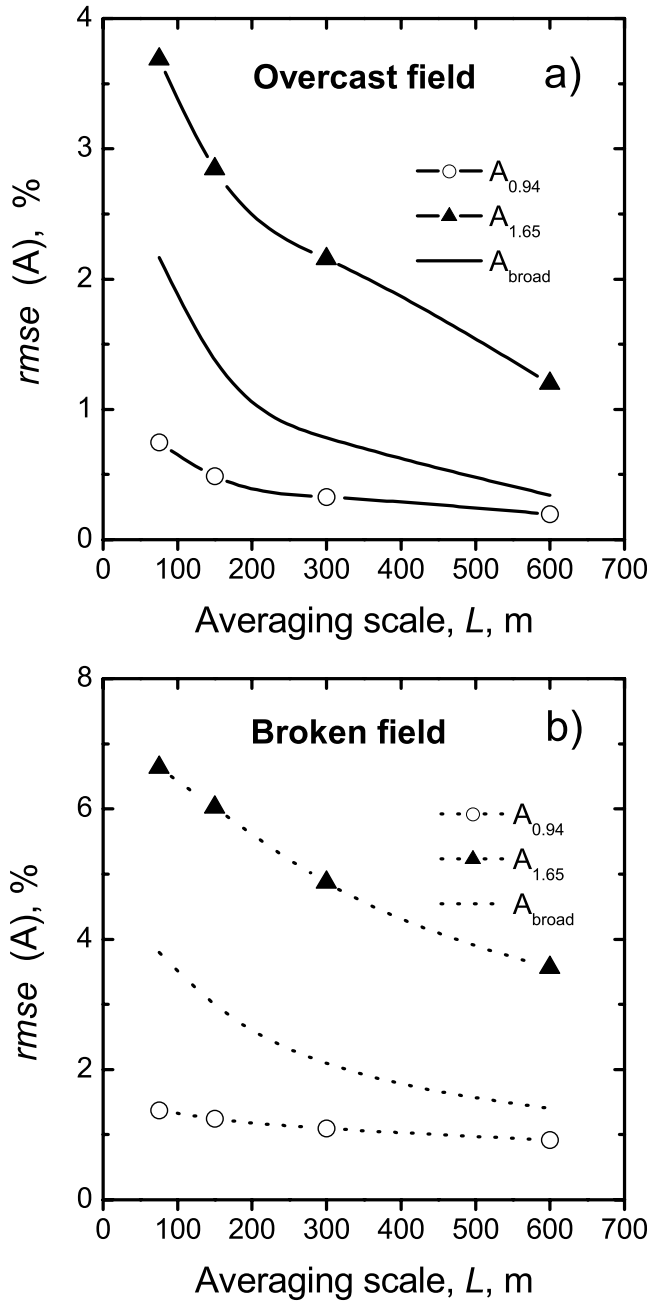


Figure 8. The effect of the spatial averaging scale L on the accuracy ($rmse$) of the spectral ($A_{0.94}$, $A_{1.65}$) and broadband (A_{broad}) absorption retrievals for overcast (a) and broken (b) cloud fields.

with the reconstructed one, $A' = 1 - R - T - E_{0.7}$ on small (~ 100 m) spatial scales. Note that the reconstructed spectral absorption and broadband absorption will be calculated using the values of horizontal transport at $\lambda = 0.7 \mu\text{m}$, i.e., in the visible spectral range. It can be obtained from (1) that $A - A' = E_{ir} - E_{0.7}$; therefore the $rmse$ error for absorption is equal to the $rmse$ error for horizontal transport. Figure 6 shows the scatterplot of A' and A at each grid column in our fine resolution simulation ($\Delta x = \Delta y = 75$ m). The differences in the slopes of the linear regressions for predicting E_{ir} from E_{vis} provide the similar differences in the

slopes of the linear regressions for predicting A from A' . Furthermore, the large scatter of points around the $E_{0.7}$ vs $E_{1.65}$ regression line leads to a large spread of points around the A vs A' regression line. The same is true for broadband values. As a result, at small (~ 100 m) spatial scales, the reconstructed absorption, A' , may diverge from the real one, A , by as much as a factor of two (Figure 6). Clearly the value of E_{vis} cannot provide a reliable estimate for the spectral and broadband absorption at small spatial scales.

[39] Let us estimate the accuracy of the retrieval on a larger spatial scale. To do this we will use radiative fluxes averaged over scales $L_x = nx\Delta x$ and $L_y = ny\Delta y$, $nx = ny = 8$. We apply nonoverlapping averaging; therefore, the number of points will be lower by a factor $nx \times ny$. The spatial averaging decreases both $var(E_{vis})$ and $var(E_{ir})$ by about 25% while having little effect on the correlation coefficient. As a result, the spread of points about the regression straight lines decreases, but the slope of the regression line between E_{vis} and E_{ir} remains the same (Figures 7a, 7b, and 7c). To get a more reliable absorption estimate, we apply both the spatial averaging and the linear regression modification (section 2). As a result, the $rmse$ error of cloud absorption retrieval can decrease by more than two times (Figures 7d, 7e, and 7f).

[40] Here we used the slope values derived for the analyzed 3-D cloud fields (Figure 1). Since the slope is a function of cloud type (see, e.g., Table 3), its value is unknown for a particular cloud field. To make the regression modification practical, the following can be suggested. First, different cloud types are defined by a few parameters (e.g., the mean and variance of optical depth). Second, the model slope values are derived for each cloud type. Third, during observations the cloud type is specified (e.g., from aircraft measurements of nadir radiance in the visible spectral range). Finally, the corresponding empirical values of slopes are applied. Note, the suggested approach is similar to that described by *Loeb et al.* [2000]: empirical angular distribution models defined for different scene types were used for estimating top-of-atmosphere albedo.

[41] The magnitude of $rmse$ error depends strongly on wavelength (Figure 8). This can be explained in terms of $var(E_\lambda)$ and ΔI^*_λ . From the theory of random processes it is known that for sufficiently long averaging spatial scale L , the variance of the sample mean $\hat{E}_\lambda(L)$ is approximately equal to $var(E_\lambda)\Delta I^*_\lambda/L$ [see, e.g., *Bendat and Piersol*, 1967]. Therefore, the sample mean $\hat{E}_\lambda(L)$ is a good estimate of the true mean $\langle E_\lambda(L) \rangle = 0$ only when the averaging spatial scale $L \gg var(E_\lambda)\Delta I^*_\lambda$. Since $var(E_\lambda)$ and ΔI^*_λ are functions of the wavelength (section 4), the accuracy of the absorption retrieval depends on the choice of the spectral interval (for given sample size L). Therefore, to get the required accuracy of absorption retrieval (e.g., for fixed $rmse$), one can use a different spatial resolution for different wavelengths (Figure 8). Specifically, for the broken field, synchronous measurement fluxes at $0.7 \mu\text{m}$ and $1.65 \mu\text{m}$ wavelengths can be applied to study quite accurately ($rmse \sim 4\%$) large-scale (~ 600 m) variations of spectral absorption, while the reliable ($rmse \sim 4\%$) estimations of broadband absorption can be obtained with a higher (~ 100 m) spatial resolution (Figure 8b). We note that the conclusions in this and preceding sections correspond to the nearly maximum fluctuations of the horizontal transport ($SZA = 60$)

and therefore to its nearly maximum influence on cloud absorption retrieval.

6. Summary

[42] A few recent studies have provided the first important demonstration of how the horizontal transport depends on the absorption by water droplets/water vapor (see section 2). The present work further evaluates the spectral dependence of the radiative horizontal transport E and its effect on the accuracy of both spectral and broadband absorption retrieval in the near-IR wavelength range. We have introduced spectral dependence of the horizontal transport E in terms of its basic statistics: the variance $var(E)$ (determines the amplitude of E fluctuations), the correlation radius Δl^* (determines the spatial scale of E fluctuations) and the correlation coefficient $\rho(E_{vis}, E_{ir})$ (measures the degree of linear dependence between values of the horizontal transport in visible E_{vis} and near-IR E_{ir} spectral range). Using observations made during the ASTEX field campaign and the LES model with explicit liquid phase microphysics, we have simulated two types of marine clouds representing inhomogeneous overcast and broken stratocumulus clouds. The radiative calculations (spectral range 0.7–2.7 μm) were performed by applying a 3-D Monte Carlo radiative transfer model. The main results are the following:

1. The spectral variations of absorbing properties (single scattering coalbedo of cloud droplets and absorption coefficient of atmospheric gases) are key factors governing the spectral behavior of E , while the spectral dependence of cloud scattering parameters (extinction coefficient and scattering phase function) is negligible. This is associated with the spectral variability of the scattering and absorbing properties. The scattering properties are almost spectrally independent. In contrast, the absorbing properties vary significantly with wavelength.

2. Two competing effects determine spectral signatures of the horizontal transport E . These two effects can be described in terms of the Monte Carlo radiative transfer technique: the presence of absorption increases the number of photon trajectories contributing to the horizontal transport (the first effect), but decreases their weight that is proportional to photon energy (the second effect).

3. Unscattered radiation, passing in gaps between clouds, can make a considerable contribution to the horizontal transport. Thus, for broken clouds, the spectral behavior of E is determined by the spectral variability of both the diffuse component and the unscattered one. The latter describes the major differences in spectral behavior of the basic statistics of E in the overcast and broken clouds. For example, the unscattered component is independent of the droplet absorption. Therefore, for the broken clouds, the correlation radius Δl^* is weakly controlled by the water droplet absorption. For overcast clouds, absorption by water droplets (1.65 μm wavelength) decreases the correlation radius Δl^* substantially.

4. Spectral variability of the variance, $var(E)$, and the correlation coefficient, $\rho(E_{vis}, E_{ir})$, define the variance of the broadband horizontal transport $var(E_{broad})$. For some wavelengths the inequality $var(E_{ir}) > var(E_{vis})$ holds, but for other wavelengths the opposite $var(E_{ir}) < var(E_{vis})$

occurs. Due to these spectral features, the broadband value of the variance $var(E_{broad})$ can be close to the visible value $var(E_{vis})$. We illustrated this for the broken case (section 4b). Therefore, small differences between broadband $var(E_{broad})$ and visible $var(E_{vis})$ values cannot be considered an indication that the variance $var(E)$ has a weak spectral dependence. The same is true for the normalized correlation function of E .

5. Spectral variability of the variance, $var(E)$, and the correlation coefficient, $\rho(E_{vis}, E_{ir})$, determine the slope of the regression line between E_{ir} and E_{vis} . As a result, the slope is spectrally dependent, and its spectral values can be less or greater than 1. If the slope spectral value is relatively large then for each increase of one unit in E_{vis} , E_{ir} will increase drastically. Conversely, if the slope spectral value is relatively small then for each increase of one unit in E_{vis} , E_{ir} will increase only slightly.

6. For given accuracy of absorption retrieval (e.g., for fixed $rmse$), the spectral/broadband absorptions can be estimated with different spatial resolution. This is mainly due to the following: (1) for accurate absorption estimation, the spatial sample size should be larger than the product of $var(E)$ and Δl^* ; (2) both the variance $var(E)$ and the correlation radius Δl^* are functions of the wavelength. For example, for the broken clouds and the fixed accuracy of retrieval ($rmse \sim 4\%$), the spectral absorption (1.65 μm) can be estimated with a maximum resolution of ~ 600 m, whereas the broadband absorption can be estimated with higher (~ 100 m) resolution.

[43] The conclusions so far were obtained for two typical fields of marine stratocumulus clouds, both nonprecipitating and drizzling. More simulations of different cloud fields/types are needed in order to provide a better understanding of the spectral and broadband variability of the horizontal transport, its dependence on averaging scale, cloud type, and hence improve cloud retrieval techniques.

Appendix A: A Monte Carlo Technique

[44] We used the method of direct simulation to calculate the absorption and radiative fluxes [Marchuk *et al.*, 1980]. A photon free path length in a cloud layer was simulated by the method of “maximal cross section.” In each n th collision event the absorption of the photon by water droplets was not simulated, but rather, the photon statistical weight was appropriately modified.

[45] The selective absorption of solar radiation by atmospheric gases is treated using transmission function $P_{\Delta\nu}(l)$, having the meaning of photon “survival” probability on the path of length l traveled by the photon from the entry point along a given trajectory Ω . The $P_{\Delta\nu}(l)$ value is determined by equivalent absorber mass, $w^*[I(\Omega)]$, on the path length l along the given trajectory Ω . We used transmission function of the form [e.g., Marchuk *et al.*, 1980; Feigelson, 1984]:

$$P_{\Delta\nu} = \exp \left\{ - \sum_{k=1}^N \beta_{\Delta\nu}(w^*)^{m_{\Delta\nu}} \right\}, \quad (A1)$$

where $\Delta\nu \sim 20 \text{ cm}^{-1}$, k is the atmospheric gas number (e.g., $k = 1$ for water vapor, $k = 2$ for carbon dioxide, $k = 3$ for ozone, etc.); N is the number of absorbing gases; $\beta_{\Delta\nu}$,

$m_{\Delta\nu}$ are empirical parameters [e.g., Feigelson, 1984]. For a given spectral interval (0.7–2.7 μm) we set $N = 2$.

[46] To treat the atmospheric gas absorption, we used the equivalence theorem [Irvine, 1964; van de Hulst, 1980] by which the gas absorption processes do not depend on the droplet scattering and absorption processes. According to this theorem, the fluxes of interest to us can be determined through the photon path length distribution function $J(l, z)$. For instance, the upward flux $F_{\Delta\nu}^{\uparrow}(z_j)$ at the vertical level z_j is given by

$$F_{\Delta\nu}^{\uparrow}(z_j) = \int_0^{\infty} J(l, z_j) P_{\Delta\nu}(l, z_j) dl, \quad (\text{A2})$$

[47] Following the general principles of evaluating integrals by the Monte Carlo method, we calculated the vertical and horizontal fluxes. To estimate the gaseous absorption in a pixel, we used the law of radiative energy conservation. Specifically, the calculated net fluxes at all (lateral, top, and bottom) faces of the pixel were summed up to give the pixel absorption.

[48] It is worth noting that (1) any available transmission function can be used in our Monte Carlo model, and (2) this model has been validated during the International Inter-comparison of 3-D Radiation Codes (I3RC) (see web page <http://climate.gsfc.nasa.gov/I3RC>).

[49] **Acknowledgments.** This work was supported by the Office of Biological and Environmental Research of the U.S. Department of Energy as part of the Atmospheric Radiation Measurement Program and ONR grants N00014-96-1-0687 and N00014-96-1-1112. We are grateful to J. Barnard and anonymous reviewers for thoughtful comments and N. Burleigh for assistance during the preparation of the manuscript.

References

- Ackerman, S. A., and S. K. Cox, Aircraft observations of the shortwave fractional absorptance of non-homogeneous clouds, *J. Appl. Meteorol.*, **20**, 1510–1515, 1981.
- Arking, A., Absorption of solar energy in the atmosphere: Discrepancy between model and observations, *Science*, **273**, 779–782, 1996.
- Asano, S., M. Shiobara, and A. Uchiyama, Estimation of cloud physical parameters from airborne solar spectral reflectance measurements for stratocumulus clouds, *J. Atmos. Sci.*, **52**, 3556–3576, 1995.
- Barker, H. W., and Z. Li, Interpreting shortwave albedo-transmittance plots: True or apparent anomalous absorption?, *Geophys. Res. Lett.*, **24**, 2023–2026, 1997.
- Barker, H. W., and A. Marshak, Inferring optical depth of broken clouds above green vegetation using surface solar radiometric measurements, *J. Atmos. Sci.*, **58**, 2989–3006, 2001.
- Barker, H. W., G. L. Stephens, and Q. Fu, The sensitivity of domain-averaged solar fluxes to assumptions about cloud geometry, *Q. J. R. Meteorol. Soc.*, **125**, 2127–2152, 1999.
- Bendat, J. S., and A. G. Piersol, *Measurement and Analysis of Random Data*, 390 pp., John Wiley, New York, 1967.
- Cess, R. D., et al., Absorption of solar radiation by clouds: Observations versus models, *Science*, **267**, 496–499, 1995.
- Cess, R. D., M. Zhang, F. P. J. Valero, S. K. Pope, A. Bucholtz, B. Bush, C. S. Zender, and J. Vitko Jr., Absorption of solar radiation by the cloudy atmosphere: Further interpretations of collocated aircraft measurements, *J. Geophys. Res.*, **104**, 2059–2066, 1999.
- Davis, A., A. Marshak, R. Cahalan, and W. Wiscombe, The Landsat scale break in stratocumulus as a three-dimensional radiative transfer effect: Implications for cloud remote sensing, *J. Atmos. Sci.*, **54**, 241–260, 1997.
- Deirmendjian, D., *Electromagnetic Scattering on Spherical Polydispersions*, 290 pp., Elsevier Sci., New York, 1969.
- Ellingson, R. G., J. Ellis, and S. Fels, The intercomparison of radiation codes used in climate models: Long wave results, *J. Geophys. Res.*, **96**, 8929–8953, 1991.
- Feigelson, E. M., *Radiation in a Cloudy Atmosphere*, 293 pp., D. Reidel, Norwell, Mass., 1984.
- Feller, W., *An Introduction to Probability Theory and Its Applications*, vol. 1, 2nd ed., 461 pp., John Wiley, New York, 1971.
- Freund, R. J., and P. D. Minton, *Regression Methods*, 261 pp., Marcel Dekker, New York, 1979.
- Goody, R. M., and Y. L. Yung, *Atmospheric Radiation: Theoretical Basis*, 519 pp., Oxford Univ. Press, New York, 1989.
- Hayasaka, T., N. Kikuchi, and M. Tanaka, Absorption of solar radiation by stratocumulus clouds: Aircraft measurements and theoretical calculations, *J. Appl. Meteorol.*, **34**, 1047–1055, 1995a.
- Hayasaka, T., T. Nakajima, Y. Fujiyoshi, Y. Ishizaka, T. Takeda, and M. Tanaka, Geometrical thickness, liquid water content, and radiative properties of stratocumulus clouds over the western North Pacific, *J. Appl. Meteorol.*, **34**, 460–470, 1995b.
- Irvine, W. M., The formation of absorption bands and the distribution of photon optical paths in a scattering atmosphere, *Bull. Astron. Inst. Neth.*, **17**, 266–279, 1964.
- Khairoutdinov, M. F., and Y. L. Kogan, A large eddy simulation model with explicit microphysics: Validation against aircraft observations of a stratocumulus-topped boundary layer, *J. Atmos. Sci.*, **56**, 2115–2131, 1999.
- Kogan, Y. L., M. P. Khairoutdinov, D. K. Lilly, Z. N. Kogan, and Q. Liu, Modeling of stratocumulus cloud layers in a large eddy simulation model with explicit microphysics, *J. Atmos. Sci.*, **52**, 2923–2940, 1995.
- Li, J., D. J. W. Geldart, and P. Chylek, Solar radiative transfer in clouds with vertical internal inhomogeneity, *J. Atmos. Sci.*, **51**, 2542–2552, 1994.
- Liou, K. N., *Radiation and Cloud Processes in the Atmosphere: Theory, Observation, and Modeling*, 487 pp., Oxford Univ. Press, New York, 1992.
- Loeb, N. G., F. Parol, J.-C. Buriez, and C. Vanbauce, Top-of-atmosphere albedo estimation from angular distribution models using scene identification from satellite cloud property retrievals, *J. Clim.*, **13**, 1269–1285, 2000.
- Marchuk, G., G. Mikhailov, M. Nazareliev, R. Darbinjan, B. Kargin, and B. Elepov, *The Monte Carlo Methods in Atmospheric Optics*, 208 pp., Springer-Verlag, New York, 1980.
- Marshak, A., A. B. Davis, W. J. Wiscombe, and R. F. Cahalan, Radiative smoothing in fractal clouds, *J. Geophys. Res.*, **100**, 26,247–26,261, 1995.
- Marshak, A., A. B. Davis, W. J. Wiscombe, and R. F. Cahalan, Inhomogeneity effects on cloud shortwave absorption measurements: Two-aircraft simulations, *J. Geophys. Res.*, **102**, 16,619–16,637, 1997.
- Marshak, A., W. J. Wiscombe, A. B. Davis, L. Oreopoulos, and R. F. Cahalan, On the removal of the effect of horizontal fluxes in two-aircraft measurements of cloud absorption, *Q. J. R. Meteorol. Soc.*, **125**, 2153–2170, 1999a.
- Marshak, A., L. Oreopoulos, A. B. Davis, W. J. Wiscombe, and R. F. Cahalan, Horizontal radiative fluxes in clouds and accuracy of the Independent Pixel Approximation at absorbing wavelengths, *Geophys. Res. Lett.*, **26**, 1585–1588, 1999b.
- Ramanathan, V., B. Subasilar, G. Zhang, W. Conant, R. Cess, J. Kiehl, H. Grassl, and L. Shi, Warm pool heat budget and short-wave cloud forcing: A missing physics?, *Science*, **267**, 499–503, 1995.
- Rawlins, F., Aircraft measurements of the solar absorption by broken cloud fields: A case study, *Q. J. R. Meteorol. Soc.*, **115**, 365–382, 1989.
- Soulen, P. F., M. D. King, S.-C. Tsay, G. T. Arnold, and J. Y. Li, Airborne spectral measurements of surface-atmosphere anisotropy during the SCAR-A, Kuwait oil fire, and TARFOX experiments, *J. Geophys. Res.*, **105**, 10,203–10,218, 2000.
- Stephens, G. L., and S.-C. Tsay, On the cloud absorption anomaly, *Q. J. R. Meteorol. Soc.*, **116**, 671–704, 1990.
- Titov, G. A., Radiative horizontal transport and absorption in stratocumulus clouds, *J. Atmos. Sci.*, **55**, 2549–2560, 1998.
- Titov, G. A., and E. I. Kasjanov, Radiative effects of inhomogeneous stratocumulus clouds, in *IRS'96: Current Problems in Atmospheric Radiation*, edited by W. L. Smith and K. Stamnes, pp. 78–81, A. Deepak, Hampton, Va., 1997.
- van de Hulst, H. C., *Multiple Light Scattering*, 739 pp., Academic, San Diego, Calif., 1980.
- Varnai, T., Influence of three-dimensional radiative effects on the spatial distribution of shortwave cloud reflection, *J. Atmos. Sci.*, **57**, 216–229, 2000.

E. I. Kassianov, Pacific Northwest National Laboratory, 902 Battelle Boulevard, P.O. Box 999, Richland, WA 99352, USA. (evgueni.kassianov@dpnl.gov)

Y. L. Kogan, Cooperative Institute for Mesoscale Meteorological Studies, University of Oklahoma, Norman, OK 73019, USA.